JOURNAL OF APPLIED ELECTROCHEMISTRY **27** (1997) 267–279

Dissolution and passivation processes in the corrosion of copper and nickel in KF.2HF at 85 °C

H. DUMONT, S.Y. QIAN, B.E. CONWAY

Chemistry Department, University of Ottawa, 10 Marie Curie Street, Ottawa, Ontario, KIN 6N5, Canada

Received 17 January 1996; revised 21 May 1996

The process of electrolytic production of fluorine is conducted in a melt of KF.2HF at about 85 °C. The metallic cell materials, copper and copper–nickel alloys (Monel), and the steel electrodes that are used as the cathode, are subject to substantial corrosion in the liquid electrolyte. Comparative studies are reported on the relative extent of corrosion of copper and nickel in the above melt, and the respective passivation behaviours of these two metals. The formation of fluoride films on the two metals is examined by means of cyclic voltammetry and complementarily through recording of open-circuit potential-decay transients, following passivation. Flade behaviour is observed and the role of diffusion-controlled processes in depassivation is quantitatively evaluated. Weight-change measurements also support the electrochemically derived results. The passive film at Ni is much less easily reducible than at Cu.

1. Introduction

In addition to their use in the process of electrolytic production of fluorine, which is the principal concern in the present paper, molten fluorides are extensively used in several other technologies: the aluminium industry employs an $AlF_3.(NaF)_3$ melt at 960 °C [1], a LiF.NaF.KF eutectic, molten above 400 °C, is used for the electrodeposition of refractory metals such as Ti, Nb [2] and NF_3 is obtained by means of electrolysis of an $NH_4F.HF$ melt [3–5] and/or of an aniline solution in HF [4]. However, despite the great importance of molten fluorides in electrochemical process technologies, little attention has been paid to the stability of various materials in fluoride melts, most probably owing to the fact that the main concerns of the fluorine and aluminium industries have been focused on the so-called 'anode effect' at the carbon electrodes used as anodes, leading to problems of reliability and efficiency of the processes, and of high anode polarization [5–7].

The study of materials in KF/HF melts presents challenging problems of a different kind in the corrosion field on account of the special properties of such media [8]. The corrosion behaviour of copper and nickel in the KF.2HF melt at 85 °C is of interest on an applied electrochemistry basis since copper, nickel and copper-nickel alloys (Monel) are supposedly fairly corrosion resistant [9,10] and for this reason are largely used in the fluorine industry. Important quantities of Cu and Ni compounds are, however, found in the industrial melt, arising from the construction materials of the cell and cause efficiency loss at the mild steel cathodes.

Hackerman, Snavely and Fiel [10] classified the corrosion behaviour of 23 metals in high purity anhydrous HF (AHF) in three groups exhibiting: (i) rapid corrosion; (ii) slow corrosion or (iii) passivation. Monel and Ni fall in this last category and Cu in the second. Vijh [11] has explained how the solid state properties of the films that are formed at corroding metals give a ready explanation for the three types of behaviour. In anhydrous HF the Hammett acidity coefficient (H_0) is −11 (meaning that AHF is 10^{11} times more acidic than aqueous HF solution [12]), and thus solvent autoprotolysis arises as in the water system according to the process:

$$3HF \rightleftharpoons HF_2^- + H_2F^+ \qquad (1)$$

The equilibrium constant of Process 1 has been evaluated from conductivity measurements as 10^{-12} [13], but could be expected to be as low as for the water system, (i.e., 10^{-14} [13]), if the HF were completely water free.

However, since the molten electrolyte used in most fluorine technologies [14] is KF.2HF, it has formally a strong basic character in the HF-solvent system and that property will obviously change the corrosion behaviour of various metals in relation to that in AHF media. In the molten state (in the absence of free HF solvent), the solvated proton (H_2F^+) concentration is expected to be negligible and the acid/base reaction should be considered [15] from the solvent system viewpoint as

$$HF_2^- \rightleftharpoons F^- + HF \qquad (2)$$

where HF is the strongest acid in the molten electrolyte medium.

The anodic behaviours of copper and nickel in KF.2HF at 85 °C are examined comparatively in the present paper; the procedures used involve mostly voltammetric and open-circuit film-breakdown measurements, as well as some weight-change determinations.

0021-891X

Many works have been reported in the literature on the anodic behaviour of copper in various solutions. In aqueous alkaline solution (OH^-/H_2O, which is closely related to the F^-/HF system, as pointed out above), copper is known to be anodically corroded as cuprous species with eventual formation of Cu_2O or $Cu(OH)_2$ [16–20]. Also, in acidic aqueous solution, dissolution first leads to Cu^+ species [21, 22] the stability of which depends on the complexing power of the anion. Cl^-, Br^-, I^- and NH_3 ligands lead to stable Cu^{2+} species [22]. However F^- which should belong to this series according to Pauling's electronegativity approach [23], has a weak complexing power for Cu^{2+} [24] owing to its hard–soft acid–base properties [10] and mostly to its very strong solvation shell in aqueous medium. That situation does not arise in the molten electrolyte [25] so that some complexing power of the F^- anion tends to be restored, leading possibly to significant increase in the stability of Cu^+ species in the KF.2HF melt; thus metastable CuF has already been suggested [26].

Anodic polarization of Ni in the analogous KOH/H_2O system initially leads to the formation of α-$Ni(OH)_2$ which is reducible only with difficulty and accumulates on the electrode surface [27]. Transition can occur to β-$Ni(OH)_2$, which can be further oxidized to NiO.OH in a chemically reversible manner [28].

2. Experimental details

2.1. *Cell*

A two-compartment Plexiglass cell was used as illustrated in [29]. It was mounted in an air thermostat set at 85 °C.

2.2. *Working electrodes*

The test electrodes were prepared from Aesar copper and nickel rods of stated purity, >99.5%, and had apparent areas 0.676 cm^2 and 0.544 cm^2, respectively.

Initial studies were made with a copper disk embedded in Epofix resin in order to ensure a reproducible and well defined surface area, and oriented vertically in the electrolyte melt. Such a setup gave good results only for the first few hours. Later, because of thermal expansion/contraction cycles, between measurements, corrosion currents arose above +0.300 V vs Cu/CuF_2 together with a tilt of the voltammogram lines (Fig. 1, dashed line) relative to the potential axis. To avoid such effects, the copper disc electrode was therefore studied using the 'hanging meniscus rotating disc (HMRD)' technique. This allowed reproducible and meaningful results then to be obtained (Fig. 1, solid line).

2.3. *Counter electrode*

The counter electrode having an area of 40 cm^2 was cut from a large porous carbon block of industrial anode material (Rhone–Poulenc). A copper rod, threaded into the carbon, provided an electrical connection.

2.4. *Reference electrode*

All potentials were measured vs the potential of a Cu/CuF_2 electrode prepared by evolving fluorine for a few seconds on a Cu wire in the same melt. This electrode was previously shown to behave very well as a reference electrode [6, 7, 30].

2.5. *Voltammetric studies*

The anodic behaviour of copper and nickel was studied by means of cyclic voltammetry, using potential

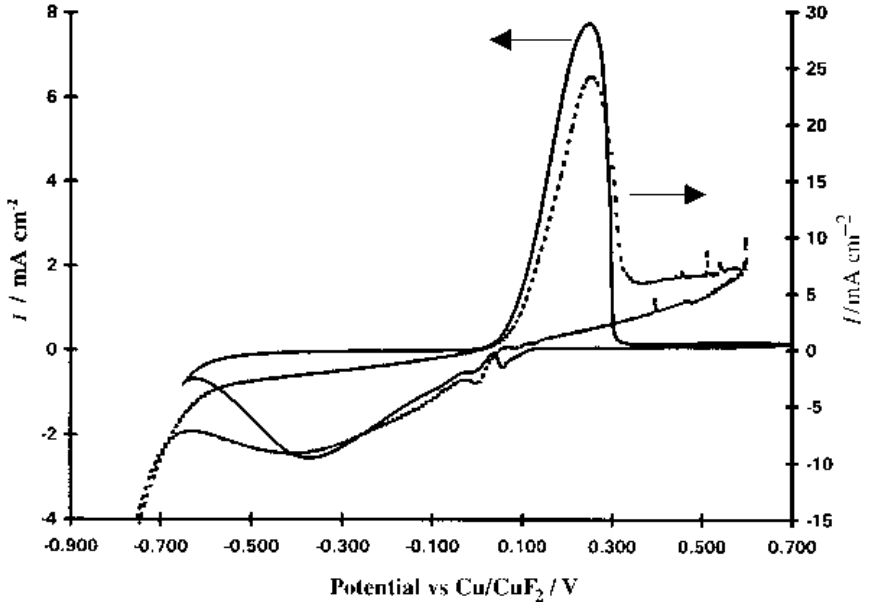

Fig. 1. Typical cyclic voltammograms for the Cu electrode in the KF.2HF melt at 85 °C, (- - - - -) with a leaking resin/metal seal and (——) with an HMRE.

scan rates between 2 and 100 mV s^{-1}, usually starting at the open-circuit potentials of Cu and Ni in the melt, viz. 0.0 V vs Cu/CuF_2 for Cu and −0.270 V for Ni. The anodic limit was 0.700 V, if not otherwise mentioned and the cathodic reverse scan was terminated before significant hydrogen evolution commenced at ~−0.650 V vs Cu/CuF_2.

2.6. *Measurements of rate of dissolution of copper fluoride passive films by recording open-circuit potential transients*

Copper fluoride films were initially grown by sweeping the potential at 20 mV s^{-1} from 0.0 V vs Cu/CuF_2 to a potential where passivation sets in: the potential was then maintained at this value for various periods of time. The final potential was generally 0.800 V vs Cu/CuF_2 or in some measurements, at 0.400 V. After the time allowed for passivation, the circuit was opened using a mercury relay and the open-circuit fall of electrode potential was recorded digitally using a Nicolet oscilloscope, model 310.

2.7. *Weight change measurements and linear polarization*

Weight change measurements were carried out in order to establish the overall corrosion behaviour of copper and nickel. The metal samples, as 2 cm × 2 cm foil pieces, were suspended in the melt. The sample preparation included degreasing in an acetone Soxhlet, chemical polishing in an appropriate acid mixture [31] and annealing in vacuum (< 10^{-4} torr) for 4 h at ~500 °C for Cu and ~600 °C for Ni.

The initially weighed samples were then held in the melt for various periods of time (from 0 to 112 days). At the end of the run, the specimens were soaked in water to remove residual melt and corrosion products, dried with acetone and then weighed a second time giving the overall weight change.

The relative rates of corrosion of Cu and Ni observed in these measurements in the KF.2HF melt at 85 °C were compared with polarization-resistance and corrosion-current data derived from linear polarization measurements conducted by recording the current responses resulting from sweeping the working electrode potential from −20 mV to +20 mV overpotential at 0.1 mV s^{-1} after an initial open-circuit immersion time of 15 min.

3. Results and discussion

3.1. *Cu behaviour in the KF.2HF melt at 85* °C

3.1.1. General considerations. Studies of the anodic behaviour of copper (as well as nickel) can be complicated by the presence of foreign electroactive impurities. The purity of the melt may be indicated in a certain way by cycling the potential over a restricted range between that for the onset of copper corrosion (0.0 V vs Cu/CuF_2) and for hydrogen evolution at ~−0.650 V vs the same reference electrode. Figure 2 shows the cyclic voltammograms for Cu in a pure KF.2HF melt (prepared from the 99+% KF.HF (solid) and 99.9% HF (liquid) by the reaction of KF.HF + HF → KF.2HF) and a melt containing an unknown impurity, most probably arising in the HF from the HF cylinder. The reversibility of the wave

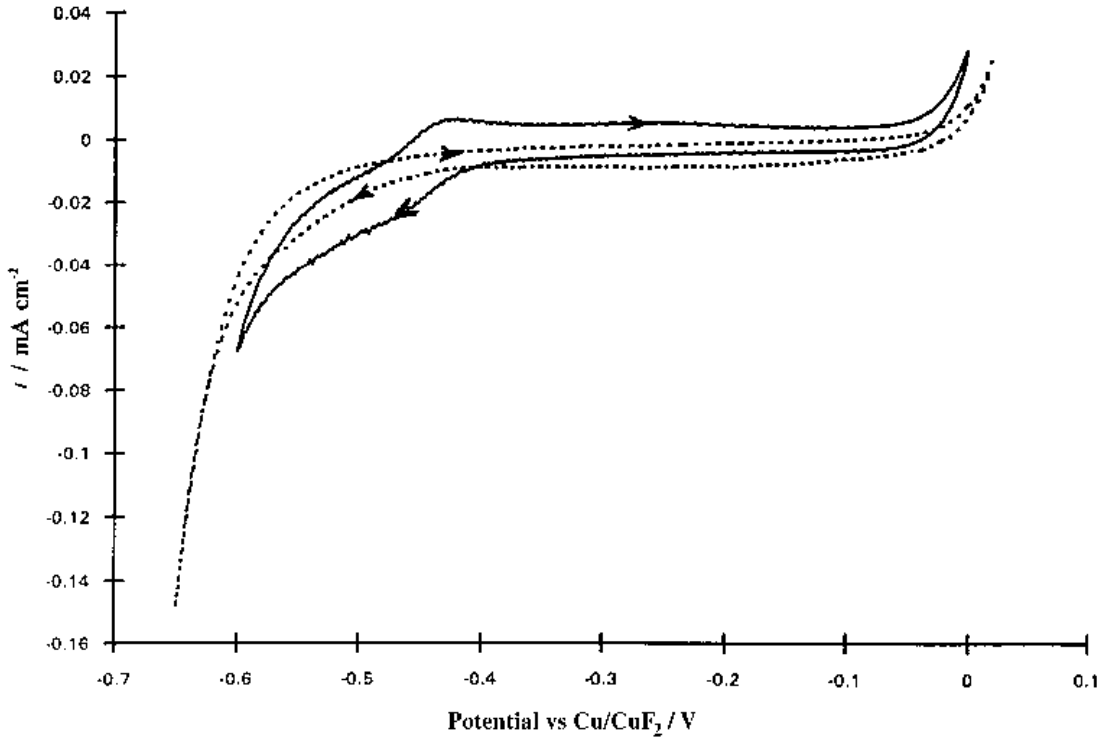

Fig. 2. Cyclic voltammogram for the Cu electrode in the impure melt (——) and in a pure melt (- - - - -) at 85 °C.

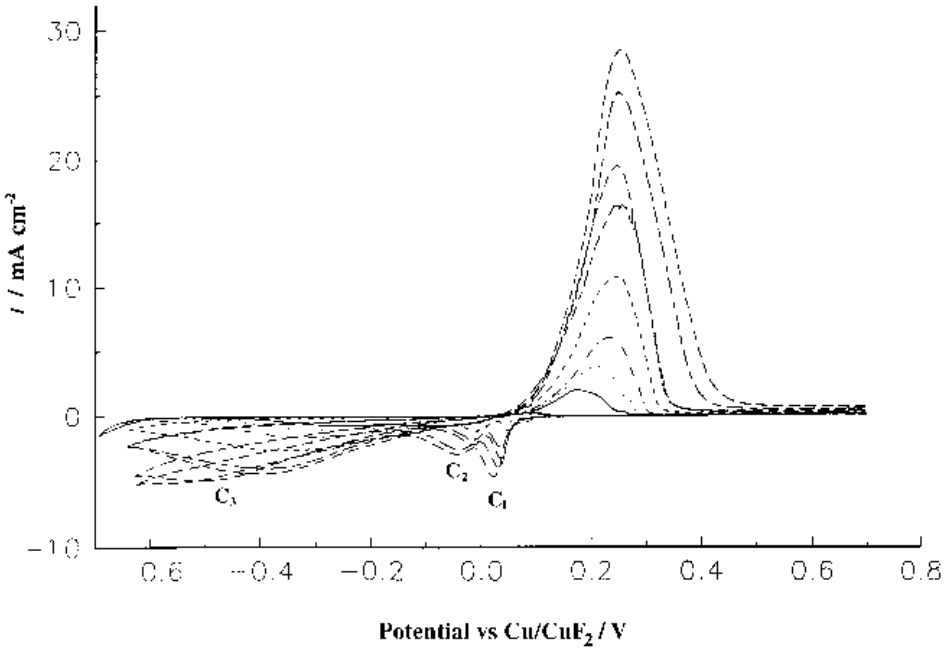

Fig. 3. Effect of scan rate on the voltammograms for Cu electrodes in the KF.2HF melt at 85 °C. Key: (——) 2, (·····) 5, (·-·-·-) 10, (- - - -) 20, (– – – –) 40, (—·—·—) 50, (– – –) 80 and (– – –) 100 mV s^{-1}.

(at −0.450 V) due to the impurity discounted water as the possible contaminant.

The cyclic voltammogram of the hanging meniscus copper electrode in pure KF.2HF melt at 85 °C at a scan rate of 10 mV s^{-1} was shown in Fig. 1. The potential scan was initiated at $E = 0.0$ vs the Cu/CuF_2 electrode in the same melt and potential was increased positively up to 0.700 V, then scanned back to reach the hydrogen potential as mentioned previously. Such voltammograms revealed an important anodic dissolution peak at ~0.250 V, beyond which the current decreased sharply with increasing positive potential, indicating that a passivating layer was being formed.

On the cathodic side, three peaks are observed at ~ +0.040 V (C_1), ~ −0.00 V (C_2) and ~ −0.400 V (C_3) (Fig. 1, solid line). The area (charge) under the cathodic peak at −0.400 V is affected by the charge under the conjugate anodic peak, while the two others seem to be affected only to much lower extents by the previously passed anodic charge which generates the passive film.

3.1.2. Sweep-rate dependence of the form of the voltammograms. Establishment of the sweep-rate dependence of an electrochemical process is of primary importance in determination of reaction mechanism, since it permits the identification of diffusion-controlled processes. In the case of NaF–AHF solution, it was established [32] that the rates of fluorine evolution are not limited by diffusion of F^- ion itself nor does it appear that this is the case for the KF.2HF melt [6]. The effect on the voltammogram of increasing the scan rate from 2 mV s^{-1} to 100 mV s^{-1} is shown in Fig. 3. In the present experiments, all four peaks observed exhibited a linear relationship between the peak-current and the square-root of the scan rate (Fig. 4) which suggests that all four processes are diffusion rather than activation limited. It should be noted that at lower scan rates a shoulder appears on the anodic side (0.270 V vs Cu/CuF_2) of the passivation peak (Fig. 3), but disappears as it is overlaid by the larger dissolution current profile at higher scan rates. This, however, suggests that the passivation is a two-step process involving a possible transmutation. Chronopotentiometry clearly showed

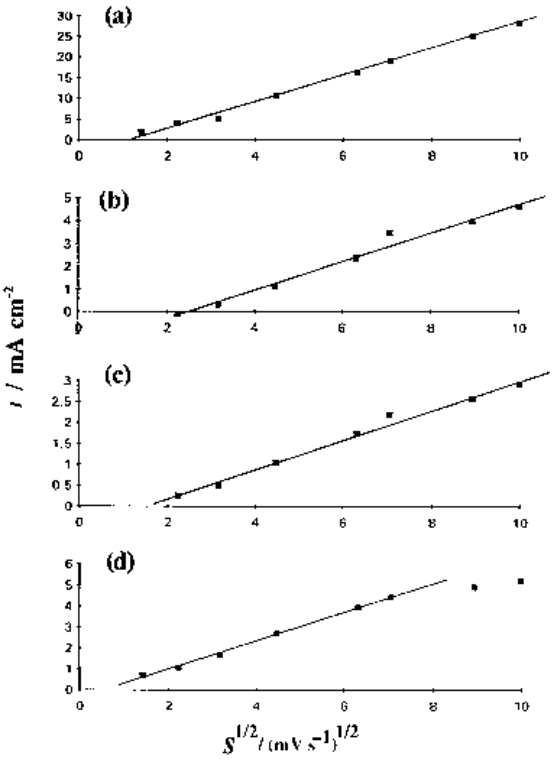

Fig. 4. The peak current density vs (scan rate)$^{1/2}$ relations for (a) the anodic peak, (b) the peak C_1, (c) the peak C_2 and (d) the peak C_3.

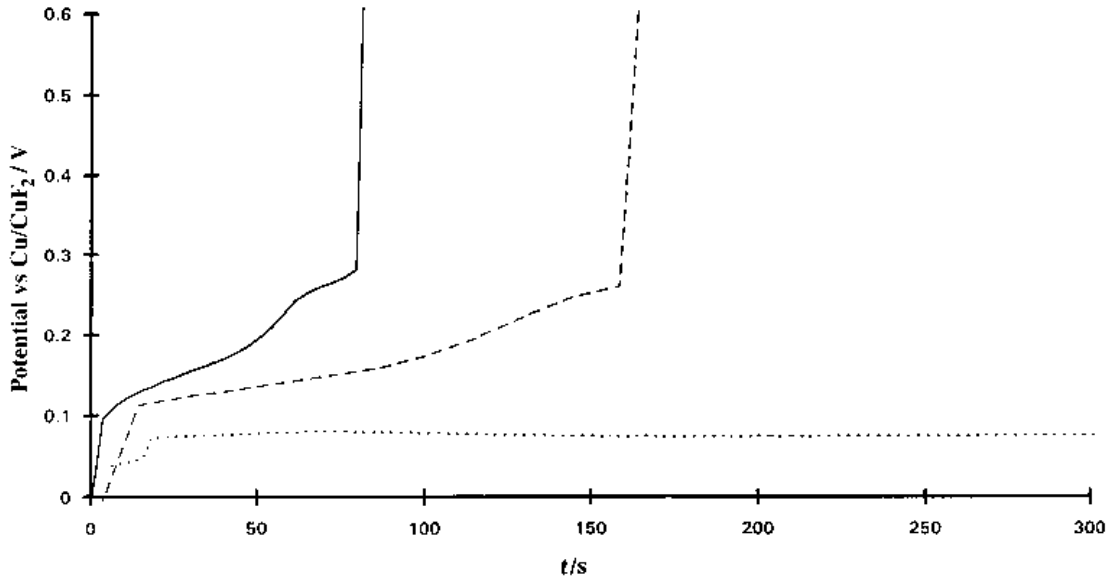

Fig. 5. Chronopotentiometry of the Cu electrode in the melt for anodic currents of (———) 1.0, (----) 0.5 and (····) 0.1 mA cm^{-2}.

(Fig. 5) that the passivation is, in fact, a two-step process with potential arrests at ~0.150 and 0.250 V vs Cu/CuF_2 for anodic currents of 0.5 and 1.0 mA cm^{-2}, respectively. However, a 0.1 mA cm^{-2} current is too low for the passivation to set in, that is, it is below the natural passivation current associated with diffusive dissolution of copper ion species.

The peak potential of the anodic peak is independent of the scan rate for values greater than 10 mV s^{-1}, (Fig. 6); below this value, the peak potential seems to have some dependence on the scan rate. This behaviour is unusual, being contrary to that commonly arising due to kinetic effects so it may be associated with formation of an insulating fluoride film. On the other hand, the potentials of the cathodic peaks (C_1, C_2 and C_3) are displaced toward less positive values with increasing scan rate (Fig. 3) which would be consistent with a kinetically limited electrochemical process such as transfer of a species through a passive film.

3.1.3. Sweep reversal experiments. Correspondence between successive anodic and cathodic processes in a voltammogram can usually be demonstrated by slowly increasing the reversal potential (E_λ) along the anodic sweep. The results of such an experiment at a scan rate of 10 mV s^{-1} are shown in Fig. 7. The inset of Fig. 7 clearly demonstrates that the broad cathodic peak is associated with the reduction of the species derived from the dissolution of copper. The cathodic peak (C_2) at ~0.0 V arises when the prior anodic sweep potential reaches 0.180 V which is very near the current maximum; the first cathodic peak (C_1) is observed when the reversal potential is ~0.280 V, that is, when complete passivation has set in and the anodic shoulder described before is observed (Fig. 7). Thus it is subsequent to the appearance of the C_2 peak.

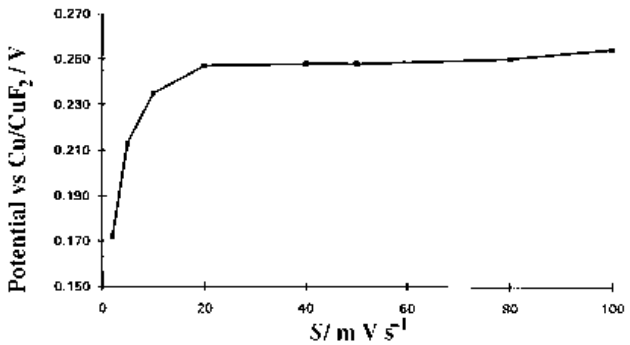

Fig. 6. Peak potential of the anodic peak against the scan rate obtained for Cu electrodes in the KF.2HF melt at 85 °C,

3.1.4. Charge considerations. As reported in Table 1, the charge (Q_a) under the anodic peak is decreased with increasing scan-rate and the total cathodic charge (Q_c) follows the same trend but with a more significant decrease leading to an increasing Q_a/Q_c ratio. Since the charges for C_1 and C_2 increase to stable values, the decrease of Q_c is mostly associated with the decrease of the charge of C_3 with increasing scan-rate. This could be ascribed to a sluggish diffusion process but the constancy of the C_1 and C_2 charges indicate a film reduction process.

3.1.5. Apparent Tafel behaviour. The number of electrons involved in the initial dissolution step may be evaluated from the voltammogram of Fig. 3, using the $dE/d(\ln i)$ slope for metal dissolution when metal cations are not initially present in solution [21, 33, 34] :

$$\frac{dE}{d\ln i} = \frac{RT}{nF} = \frac{71\,\text{mV dec}^{-1}}{n} \quad \text{at} \quad 85\,^{\circ}\text{C} \qquad (3)$$

$dE/d\ln i$ (close to 59 mV s^{-1}) is almost independent of the scan-rate, and the n values derived using Equation 3 are given in Table 2. The value of n for dissolution of Cu is thus calculated to be nominally 1 (i.e ~1.2, Table 2), suggesting that the corroding Cu is

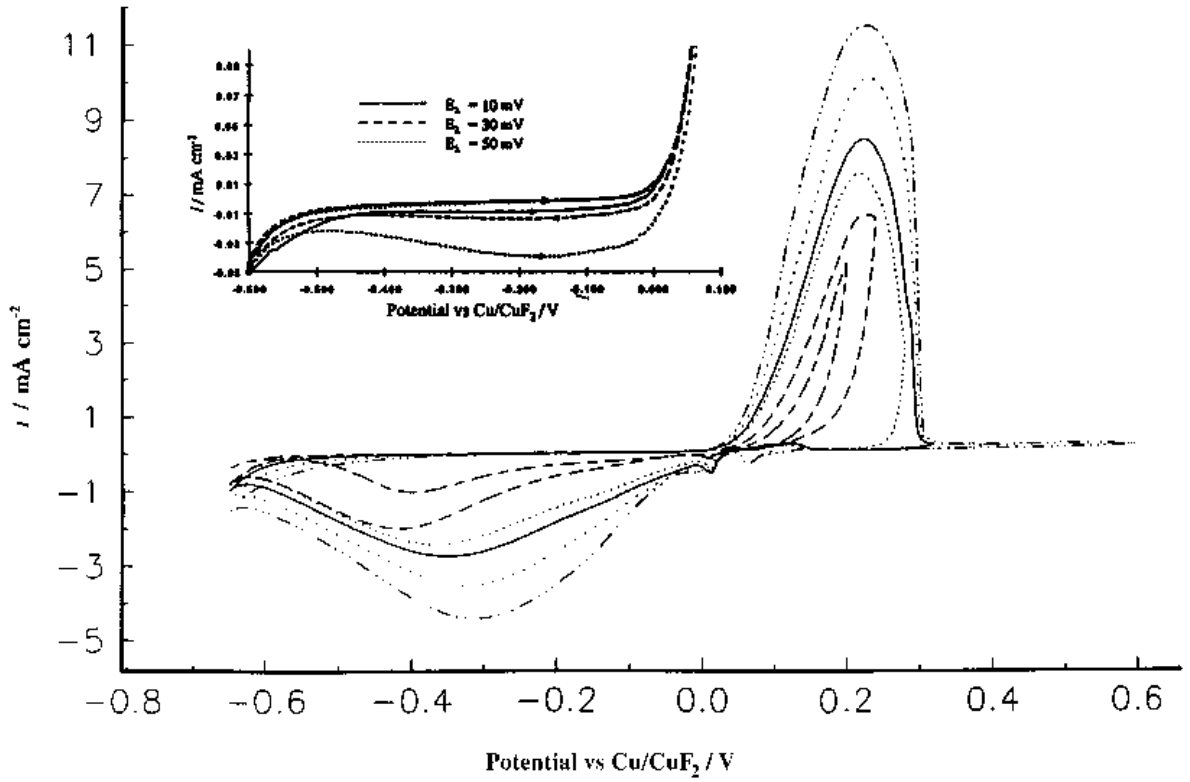

Fig. 7. Cyclic voltammograms with different anodic limit potentials (E_λ) for the Cu electrode in the KF.2HF melt at 85 °C. Inset for low anodic limits of 10, 30 and 50 mV vs Cu/CuF_2. E_λ: (–––) 0.200, (- - - -) 0.240, (·····) 0.280, (—) 0.340, (·–·–·) 0.400 and (·––·––·) 0.600 V.

dissolved as Cu^+ species in a first step. Similar dE/d ln$i$ values have been observed for copper dissolution in other media [17, 35] and at temperatures ranging from 25 to 100 °C [36, 37].

3.1.6. Assignment of cathodic current peaks based on voltammetric studies. Results presented above have related the cathodic peak (C_3) at −0.400 V to the reduction of the species that have arisen due to the initial anodic dissolution of corroding Cu which, from the apparent Tafel slope, are probably Cu^+.

As concluded in Section 3.1.4, the constancy of the charge under C_1 and C_2 with increasing scan-rate provides evidence that those two peaks are related to film reduction processes. The fact that the charges under each of them are similar and follow the same trend with regard to scan-rate also suggests that the two peaks represent successive steps that lead to complete film reduction. In the sweep reversal experiment, the C_2 peak appears when the anodic potential reaches ~0.180 V on a stationary meniscus electrode (Fig. 7, Section 3.1.3). Since, at this potential, dissolution is actively proceeding, and because various chronoamperometry experiments showed that after some periods of time (depending mostly on the state of surface roughness), the electrode can evidently become passivated at a potential around 0.150 V (dissolution–precipitation mechanism), the C_2 peak is probably associated with the reduction of copper species that have formed a film on the electrode, possibly a cuprous salt precipitated from the saturated solution near the electrode surface.

It is found that this film could be further oxidized with increasing positive limit of potential scanning, at which point complete passivation is achieved with the anodic formation of CuF_2 which corresponds to the appearence of the C_1 peak. This second oxidation step of the film is related to the shoulder observed at

Table 1. Charges associated with the different peaks as a function of scan rate for the Cu electrode in KF.2HF melt at 85 °C

Scan rate /mV s^{-1}	Q_{anode} /mC cm^{-2}	Qc_{tot} /mC cm^{-2}	Q_{anode} /Qc_{tot}	Qc_1 /mC cm^{-2}	Qc_2 /mC cm^{-2}	Qc_3 /mC cm^{-2}
2	193.5	193.2	1.001	–	–	193.2
5	143.9	119.7	1.202	–	–	119.7
10	116.0	93.1	1.246	1.18	2.37	89.6
20	110.1	87.9	1.252	2.13	3.08	82.7
40	92.5	65.6	1.410	2.52	3.11	60.0
50	84.5	59.4	1.422	2.49	3.12	53.8
80	71.1	40.7	1.748	2.31	3.25	35.1
100	74.0	33.3	2.224	2.49	2.90	27.9

Table 2. dE/d ln i relation and the number of electrons, n, involved in the anodic dissolution of Cu in KF.2HF at 82 °C

Scan rate /mV s^{-1}	*dE/d ln i* $20 < E < 100$ mV/mV dec^{-1}	*dE/d ln i calculated for n = 1 at 82 °C*	*Experimental apparent values of n*
2	58.5	70.1	1.20
5	57.7	70.1	1.21
10	58.7	70.1	1.19
20	58.7	70.1	1.19
40	59.9	70.1	1.17
50	59.2	70.1	1.18
80	56.1	70.1	1.25
100	55.3	70.1	1.27

0.280 V seen on voltammograms taken at low scan rate and corresponds with X-ray diffraction (XRD) results [5] that indicate the CuF_2 is formed anodically on Cu in 1 M KF in anhydrous HF. Thus, the cuprous species already on the surface and in the solution are oxidized to the cupric state, giving eventually the expected CuF_2 film. Hence, the C_1 peak corresponds to the initial reduction step of this CuF_2 film.

This allows the following processes for the three cathodic peaks to be respectively proposed: The C_1 peak corresponds to the reduction step:

$$Cu(II)F_{2(surf.)} + e^- \rightleftharpoons Cu(I)F_{(sol.)} + F^- \quad (4)$$

which is influened by the diffusion of Cu(I)F as follows from the square-root dependence of i_{peak} of C_1 on sweep-rate, with some kinetic effect associated with the observed dependence (Fig. 3) of E_p on scan-rate, most likely involving a resistive film of $Cu(II)F_2$ in Reaction 4. Then Cu(I), freshly produced on the electrode surface, is further reduced to Cu(0) (peak C_2), giving a similar charge as may be deduced from integration of the current profile C_1 and C_2:

$$Cu(I)F_{sol.} + 1e^- \longrightarrow Cu(0) + F^- \quad (5)$$

a process which is purely diffusion-controlled as indicated by the relations of i_{peak} and E_p to the square-root of sweep-rate.

At this point the soluble copper species in the bulk of the melt may start to be reduced, giving rise to the broad C_3 peak which was also attributed to a diffusion-controlled process according to the observed relation of i_{peak} to the square-root of scan rate.

3.1.7. Anodic dissolution mechanism suggested by the voltammetric measurements. Based on the above results and analysis, a dissolution mechanism can be proposed as follows:

$$Cu(0)_{surf.} \longrightarrow Cu(I)_{sol.} + 1e^- \quad (6)$$

$$Cu(I)_{sol.} \overset{k_{sp}}{\rightleftharpoons} Cu(I)_{surf.} \quad (7)$$

$$Cu(I)_{surf.} \longrightarrow Cu(II)_{surf.} + 1e^- \quad (8)$$

A similar mechanism was proposed for corrosion of copper in the KOH/H_2O system [14–18].

3.1.8. Open circuit potential decay and the law for growth of the passive film. The dissolution–precipitation mechanism proposed above can be verified from open-circuit potential (OCP) measurements of the rate of dissolution [38] of the passive film.

The potential decay transient that can be recorded following passivation is generally composed of three distinguishable sections. First a fast exponential decay, associated with potential relaxation through self-discharge of the double-layer capacitance, leads to an intermediate arrest potential. This arrest potential, first observed by Flade [39], is ascribed to the reversible potential of M/M^{z+} in M^{z+} saturated solution [38] (in the case of Cu in KF.2HF, the Cu/CuF_2 potential). The duration of this arrest is related to the enrichment of Cu ions in solution near the electrode brought about by dissolution of the passive film, and is thus determined by the charge for previous film formation or its thickness [40], and could be used to determine the law of film growth by determining the dissolution times following passivation for various durations. After this transition time, a sudden decrease of potential (second section) is observed and a final plateau (third section) potential is reached which depends on the bulk concentration of the Cu ion.

The Cu electrode was polarized at 0.4 V and 0.8 V vs Cu/CuF_2 (in the passive range), that is, at potentials both below and above that for the transpassive dissolution process clearly observable on voltammograms obtained at the HMRD electrode [41]; open-circuit potential decay curves for Cu recorded at various passivation times at 0.4 V are plotted in Fig. 8. The thickness of the passive film evidently increases with polarization time at this potential as might be expected.

The growth of oxide films formed on various metals usually follows either a so-called 'direct' or an 'inverse' logarithmic law in time (t). The basis of the latter law is that film growth is driven by the interphasial field (dV/dL) along the film thickness, L, and thus decreases with increasing L. This led Mott and Cabrera [42–45] to the following relation:

$$q^{-1} \propto \log(t/d^2) \quad (9)$$

where q is the film charge corresponding to a film thickness, d. On the other hand, the direct law is obtained from the formal law of anodic or atmospheric film growth [46] where q is a function of time:

$$\frac{dq}{dt} = k\exp(-Lq) \quad (10)$$

Integrating and reorganizing Equation 10 gives

$$q = \frac{1}{L}\ln kL + \frac{1}{L}\ln\left[t + \frac{\exp(Lq_0)}{kL}\right] \quad (11)$$

from which the extent of film growth, related to q, is linear with ln t when $t >> \{\exp(Lq_0)\}/kL$, where q_0 corresponds to the extent of film formation at $t = 0$. Figure 9 shows that the relation between the film thickness (or more exactly the dissolution time) and the log of polarization time is perfectly linear sug-

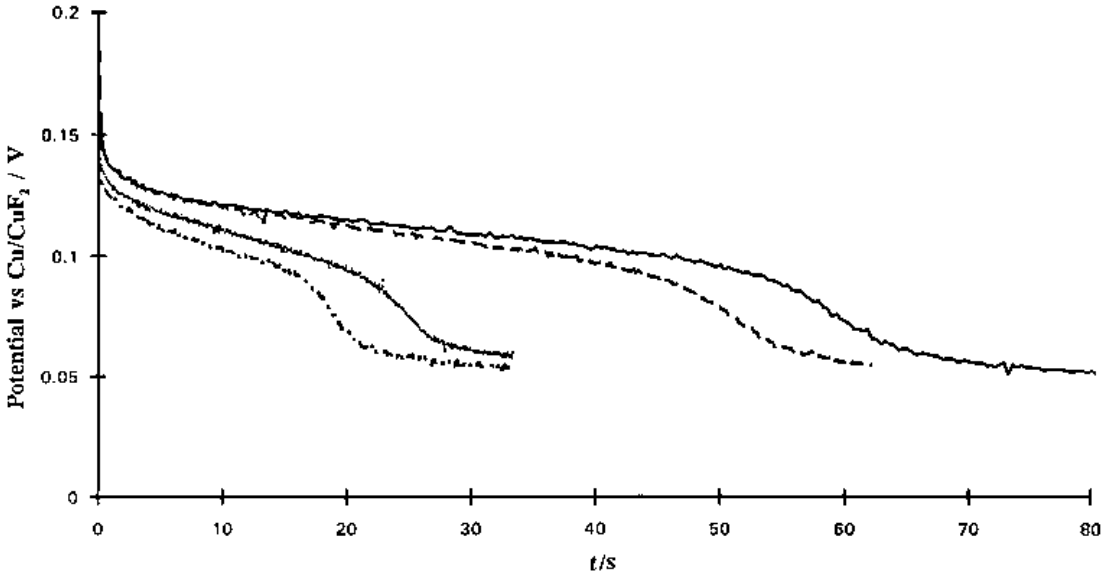

Fig. 8. Open-circuit potential decay at the Cu electrode in the melt after passivation at 0.4 V vs Cu/CuF_2 for various indicated times: (——) 180, (– –) 90, (·····) 30 and (– - –) 5 min.

gesting that the film growth follows the direct logarithmic law. On the other hand, at 0.8 V, the film thickness does not increase with the passivation time as is shown by the *constancy* of the dissolution time around 38 s (Fig. 10). However, at this potential, above the transpassive dissolution potential, the current is still relatively large (~ 140 μA cm^{-2}), which suggests that continuous dissolution takes place through a stable Cu fluoride film of virtually constant (steady-state) thickness. The dissolution rate should be similar to the diffusion rate of the soluble species in order to lead to the situation of a film either thickening or dissolving.

The Flade potential is quite similar to the reduction potential of the CuF_2 film in the cathodic C_1 peak (see Figs 3, 8 and 10), as is to be expected.

3.1.9. Relation between self-dissolution rate and the appearance of film reduction peaks on the cyclic voltammograms. Analysis of the open-circuit transients clearly shows that the self-dissolution of the passive fluoride films on Cu is fast. The dissolution rates corresponding to the behaviour shown in Fig. 10 provide evidence that the C_1 and C_2 peaks (Fig. 3) are related to the film reduction process; film dissolution would also explain the absence of a cathodic peak on the cyclic voltammograms for Cu recorded at low scan-rates (SR).

According to Shoesmith and Lee [40], the longer a passive film is allowed to become dissolved, the smaller is the charge for film reduction. For Cu, after 1 h of passivation at 0.8 V, the dissolution time is ~38 s, and considering that dissolution may commence

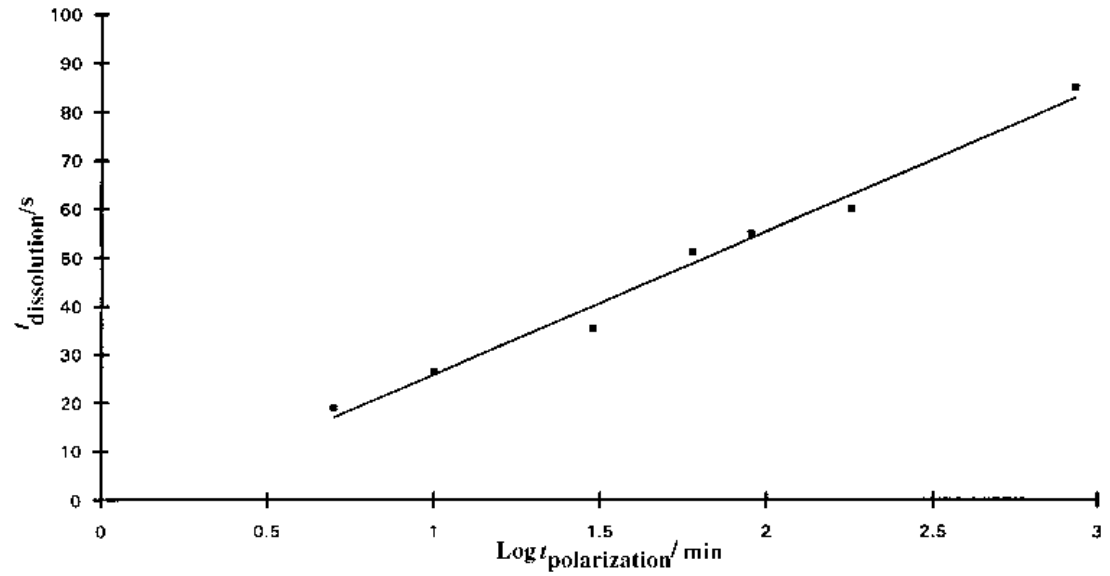

Fig. 9. The dissolution time against log of polarization time for the CuF_2 film formed at 0.4 V vs CuF_2.

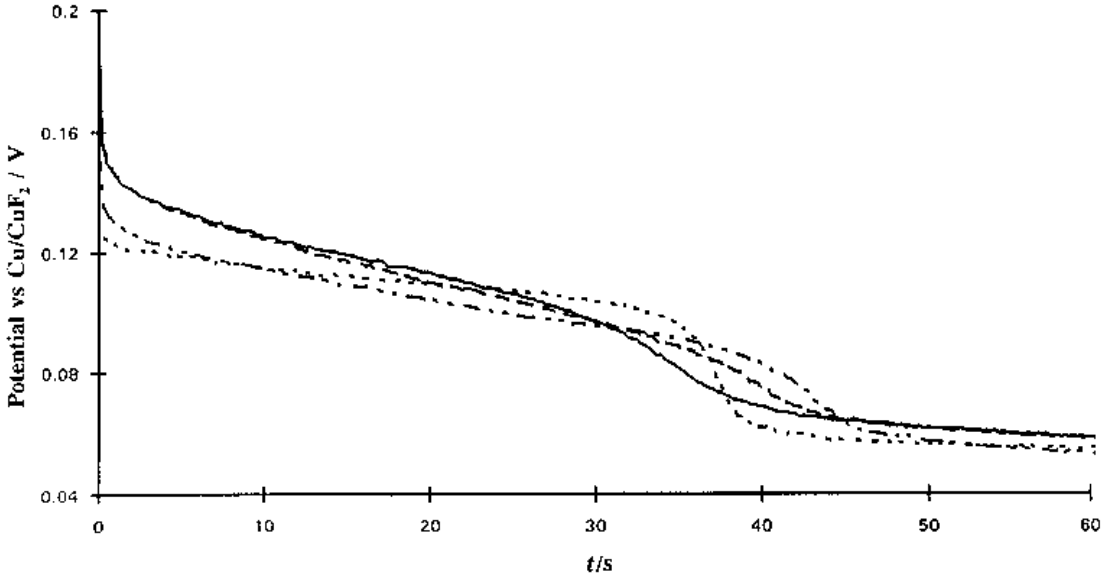

Fig. 10. Open-circuit potential decay at the Cu electrode in the melt after passivation at 0.8 V vs Cu/CuF_2 for various indicated times: (····) 30, (– – -) 300, (——) 1800 and (– –)7200 s.

just below the passivation potential, around 0.300 V (slightly SR-dependent), the reduction peak potential of the film on the cyclic voltammogram at 0.080 mV would be observed only if this potential range is covered within that period of 38 s. The SR that would ensure that the 220 mV range between the passivation and reduction potentials be covered in <40 s for Cu, in the example discussed here, should be higher than 220/40 (i.e. 5.5 mV s^{-1}). If the SR is less than the above value, the film will have become dissolved before the reduction potential is reached and anodic dissolution will then resume on the cathodic scan (see the anodic peak on the cathodic scan in Fig. 11). Figure 11 shows that this is actually the case for the CuF_2 film; when the SR is 2 mV s^{-1} or 5 mV s^{-1} (curves 1 and 2), anodic dissolution appears on the cathodic scan, but, for a higher SR of 10 mV s^{-1} (curve 3), cathodic reduction of the film becomes observable on the cyclic voltammogram. Curve 4 of Fig. 11 shows the appearance of the peak for cathodic reduction of the film when the anodic SR was 2 mV s^{-1} (the cathodic peak being usually not observed at this scan rate) and then the cathodic current response is observable at 100 mV s^{-1}. Note that resolution of the two peaks is not achieved in this case, possible because of a change in film structure or stability of the film when it is formed at a lower anodic SR. These results are consistent with the film dissolution time referred to earlier in this paper, and it is seen that the charge corresponding to film reduction should be recovered almost completely at a sufficiently high SR (Table 2).

The voltammetry results make it clear that the C_1 and C_2 peaks observed at Cu are related to the presence and behaviour of the passive film. The charge measured reaches a stable value at a sufficiently high SR and corresponds to 20 monolayers of CuF_2 as derived from the Q_{exp}/Q_{calc} ratio, 'Q calculated' being 4.98×10^{-4} C cm^{-2} for the more dense, (1 0 0), face of the Cu (f.c.c.) crystalline structure, allowing transfer

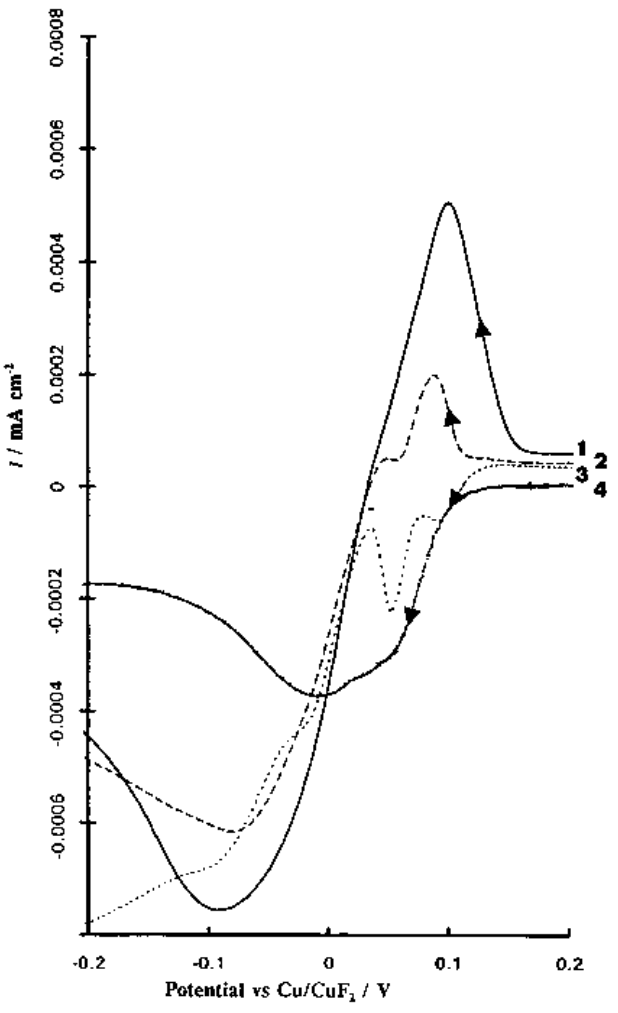

Fig. 11. Appearance of the cathodic peak current for the Cu fluoride film reduction with increasing scan rate (1: ——) 2, (2: – – – –) 5, (3: - - - -) 10 and (4: ——) 100 mV s^{-1}.

of one electron for each of the processes corresponding to the peaks C_1 and C_2, that is there is a Cu^+ intermediate species formed (Equation 6) in the overall $2e^-$ reduction.

3.2. *Anodic behaviour of Ni in the KF.2HF melt.*

The anodic behaviour of Ni in KF.2HF at 85 °C is presented here for the purpose of comparison with Cu to establish a parallel in the anodic behaviour of these two component metals of Monel in the KF.2HF melt with the work of Hackerman, Snavely and Field [10] in the more acidic AHF medium and in relation to actual Cu–Ni alloys such as Monel used for construction of plant cells.

3.2.1. Sweep reversal experiments. The voltammetric behaviour of the nickel electrode at successively increasing positive potentials was studied and the results of experiments conducted at a SR of 5 mV s^{-1} are shown in Fig. 12. The freshly polished electrode was first scanned anodically to −220 mV (solid line) and the cathodic sweep was almost coincident with the anodic one. On the second cycle (dotted line), the currents are slightly higher than on the first cycle on the anodic scan; the electrode surface roughness may have been increased by dissolution on the first cycle. However, on the reverse (cathodic) scan, the currents are significantly larger than on the anodic scan; this is typical for a nucleation process which corresponds to an auto-catalytic effect on the electrochemical reaction involved [47, 48]. This result also clearly demonstrates that initial dissolution of Ni is a prerequisite to the onset of nucleation. Thus, the effect of Ni fluoride nucleation and growth on the electrochemical dissolution should be related to the more important consumption of Ni cations near the electrode surface, as nucleation acts as a sink for Ni^{2+} ions which will largely increase the dissolution current (cf. Fig. 12) compared to that for a simple diffusion-controlled removal process.

NiF_2 nucleation was further investigated by recording current transients for potential pulses from −0.305 V to a range between −0.21 and −0.12 V vs CuF_2. Potentiostatic current transients for the nucleation of NiF_2 onto a Ni electrode in the melt are shown in Fig. 13 and exhibit a potential-dependent increase of the current after an induction time. The resulting experimental line indicates that the induction time decreases with increasing anodic potential.

The significant currents measured in this experiment suggest that the dissolution current is much greater than the rate of consumption by the NiF_2 growth process. After longer times the dissolution reaction is slowed by film formation and eventually final passivation is achieved by the deposition of NiF_2 diffusing from the solution as Ni dissolution is becoming harder. This final diffusion of NiF_2 leads to a decrease of current according to a Cottrell decay. We can observe (Fig. 13) two diffusion regimes in this decay, probably associated initially with the diffusion of Ni ions from the more concentrated region near the surface (fast regime) and then from the bulk of the melt (slow regime), the residual current being the passivation maintenance current.

3.2.2. Sweep-rate dependence of the voltammetric behaviour. The overall anodic behaviour of nickel in the melt was studied by means of cyclic voltammetry, as in the case of Cu. Scan rates were chosen between 2 and 50 mV s^{-1}, starting at the open-circuit potential of Ni in the melt. Figure 14 shows the cyclic voltammogram for the hanging-meniscus Ni electrode in the KF.2HF melt at 85 °C. It can be seen that a large anodic peak arises between ~ 0.28 to 0.47 V (depending on the sweep-rate). At more positive potentials, the currents decrease to very small values, the so-called passivation maintenance current (a few μA),

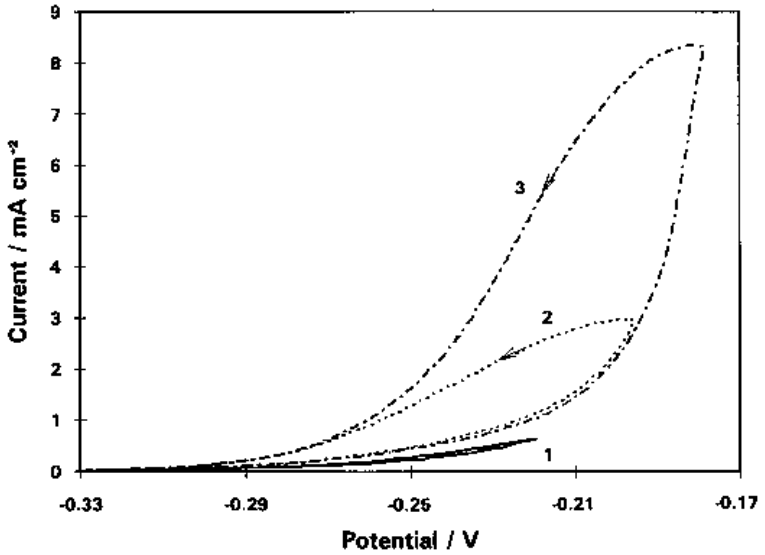

Fig. 12. Cyclic voltammograms with different anodic limit potentials, E_λ, for the Ni electrode in the KF.2HF melt at 85 °C: (——) $E_\lambda = -0.220$ V, (· · · ·) $E_\lambda = -0.195$ V, (-·-·-) $E_\lambda = -0.180$ V vs Cu/CuF_2.

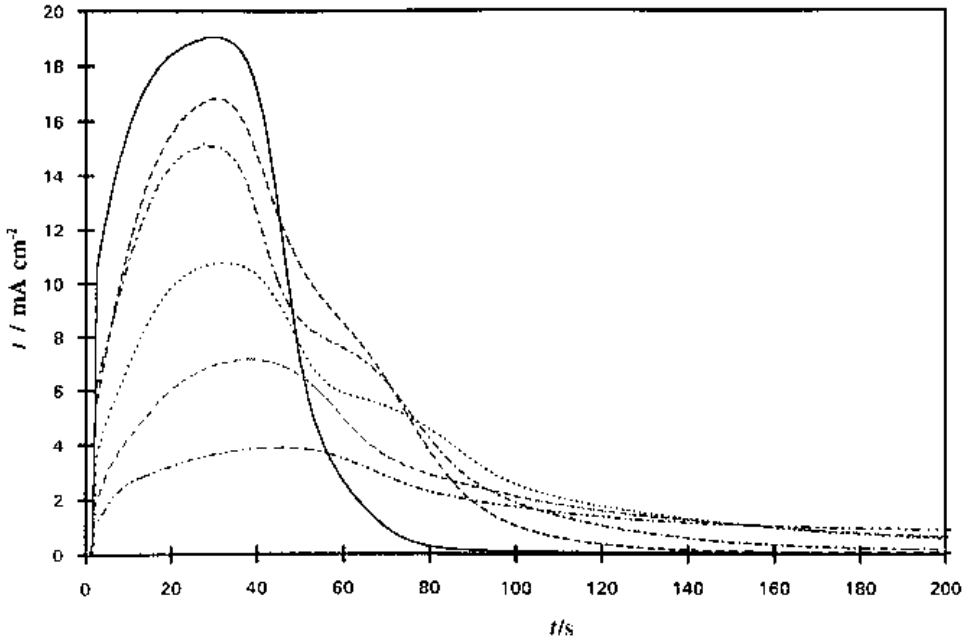

Fig. 13. Potentiostatic curent–time transients recorded after application of potential pulses from E_i = −0.305 V to −0.21 (·· ··), −0.20 V (~~~), −0.18 V (----), −0.16 V (~ · ~ · ~), −0.14 V (----) and −0.12 V (——).

indicating that a passive film had been formed. When the electrode was scanned cathodically back, no cathodic current peak for film reduction could be observed, unlike the behaviour at Cu (see Fig. 3).

The scan-rate dependency of the peak-current (Fig. 14, inset) indicates that the passivation process is diffusion-controlled in agreement with results obtained at a Ni rotating electrode. Also the higher is the SR the more positive is the passivation potential showing that passivation is determined by the rate of formation of Ni ions, and is not happening at a specific oxidation potential.

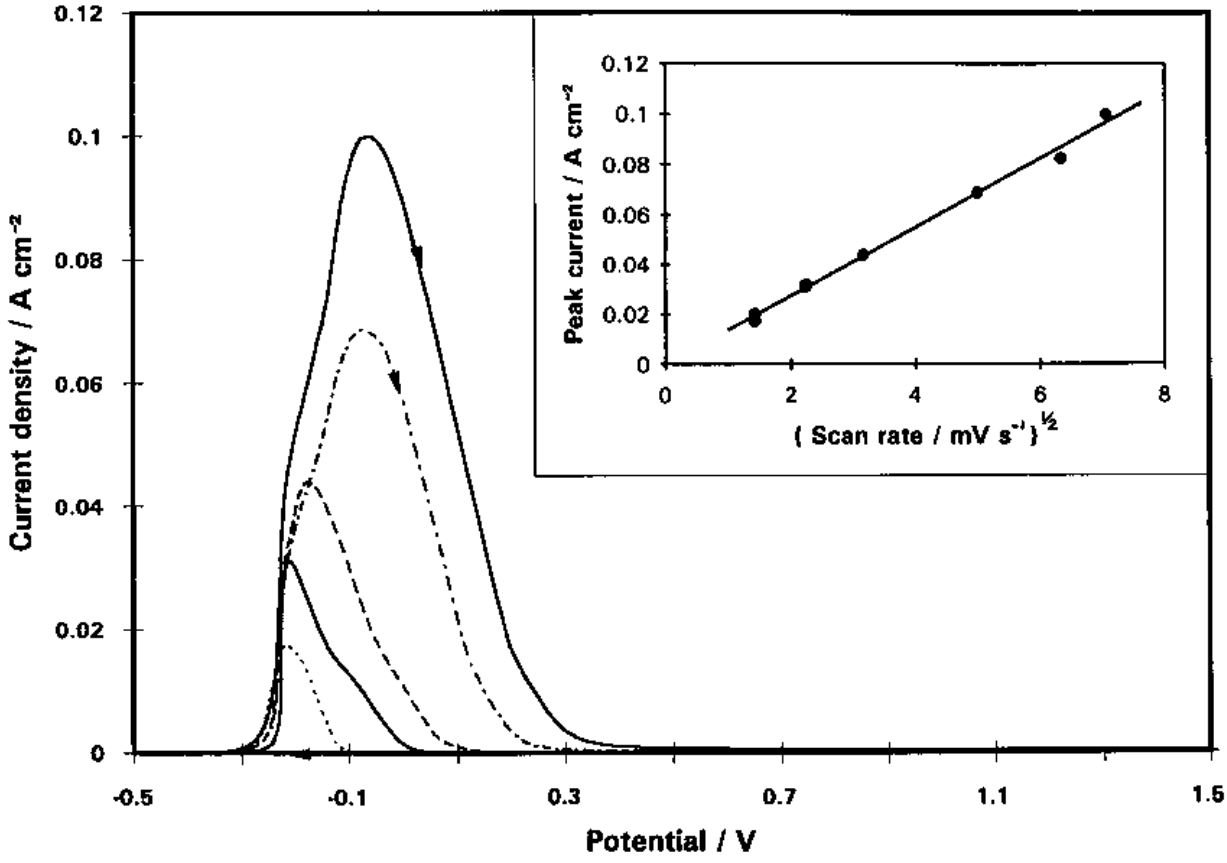

Fig. 14. Effect of scan rate on the voltammograms obtained for Ni electrodes in the KF.2HF melt at 85 °C. Inset: the I_{peak} against (scan rate)$^{1/2}$ relation for the anodic dissolution peak. Scan rate: (·····) 2, (——) 5, (– – – –) 10, (–·–·) 25 and (——) 50 mV s^{-1}.

3.2.3. Proposed mechanism for dissolution and passivation of Ni in KF.2HF at 85 °C. After an initial dissolution of Ni as Ni^{2+}, the Ni ions reach saturation near the electrode surface leading to a spontaneous nucleation with fast growth of nuclei; this causes rapid removal of Ni ions causing increase in the dissolution rate. The passivation mechanism thus involves competition between diffusion of Ni ions from the electrode and the nucleation process, as represented by

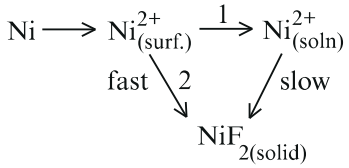

(12)

3.3. *Weight-change and linear polarization measurements*

The results of weight-change measurements conducted during a period of 112 days of electrode immersion in KF.2HF at 85 °C are reported in the Table 3. Visible solid corrosion products accumulated along the hanger outside the melt on both the copper and the nickel samples and, on the latter, a massive green deposit was formed which probably accounts for the early weight gains observed after seven days on Ni and 14 on Cu. These soluble deposits were carefully removed by adequate washing in water. Table 3 shows that weight loss is continuously increasing during the 112 days of the experiment for both metals, indicating that no complete passivation is attained. The corrosion rate on open-circuit is obtained by dividing the weight loss per cm^2 by the total period of time. Thus, for the 112 days, the mean rate of corrosion of Ni was 0.41 μg cm^{-2} h^{-1} and of Cu, 0.13 μg cm^{-2} h^{-1}. The corrision current-densities derived from the linear polarization measurements, 1 μA cm^{-2} and 10 μA cm^{-2}, respectively, for Cu and Ni are consistent with the measurements on rates of weight change.

Table. 3. Percentage weight change of Cu and Ni electrodes immersed in the melt at 85°C.

Time/days	*% weight change per cm^2 at Cu*	*% weight change per cm^2 at Ni*
1	0	0
7	0	+ 0.004
14	+ 0.013	– 0.125
35	+ 0.163	– 0.375
91	– 0.375	– 0.525
112	– 0.288	– 1.163
112	– 0.338	– 1.063
112	– 0.423	– 1.063

3.4. *Resistivities of the passive films on copper and nickel*

That the low rate of corrosion of copper in AHF [10] is related to the small electrical conductivity of the passive film formed on copper is confirmed in the present work in KF.2HF by measurements of the resistance between the working and reference electrodes using high frequency impedance spectroscopy at a potential below (–0.200 V) and above the potential at which the passivation peak arises (0.400 V). The measured resistance before the passive film had been formed was 6.6 ± 0.1 Ω, and after, it became increased to 9.2 ± 0.3 Ω, the difference being obviously due to the film resistivity.

In the case of Ni in AHF [10], the film was shown to be quite conductive. Using the same approach as for Cu, our resistivity measurements below and above the passivation potential, showed no significant change, the film being thus conductive.

4. Conclusions

The anodic behaviours of copper and nickel, investigated in KF.2HF melts at 85 °C, are significantly different. In the case of Cu, the passivation process involves two electrochemical steps leading to a Cu(II) fluoride passive film about 20 monolayers in thickness. The times for dissolution of the CuF_2 passive films provide a means of following the prior film growth which was found to follow the direct logarithmic law in polarization time.

The anodic behaviour of Ni involves a well defined process of nucleation and growth of $Ni(II)F_2$ from a saturated Ni ion boundary layer. The electrochemically grown passive film on Ni was, however, irreducible at potentials less negative than that for hydrogen evolution, unlike the situation for passive film reduction at Cu.

The resistivity of the passive film on Cu is high, while the passive film on Ni is quite conductive and prevents Ni dissolution. The current for maintenance for passivation is lower on Ni than on Cu in the KF.2HF melt.

5. Acknowledgements

Grateful acknowledgement is made to Cameco Corporation, Canada and the Natural Sciences and Engineering Research Council of Canada for financial support of this work. Special thanks are due to Dr D. G. Garratt of Cameco Corp. for many useful discussions.

6. References

[1] S. S. Djokić, B. E. Conway and T. F. Belliveau, *J. Electrochem. Soc.* **141** (1994) 2103.
[2] A. Robin and J. De Lépinay, *Electrochim. Acta* **37** (1992) 2433.
[3] O. Ruff, J. Fisher and F. Luft, *Zeit. Anorg, Allg. Chem.* **172** (1928) 417

[4] C. B. Colburn in *Advances in Fluorine Chemistry*, M. Stacey, J. C. Tatlow and A. G. Sharpe (Eds), Butterworths, London, vol. **3** (1963).
[5] A. Tasaka, K. Miki, T. Ohashi, S. Yamagushi, M. Kanemaru, N. Iwanaga and M. Aritsuka. *J. Electrochem. Soc*. **141** (1994) 1460.
[6] L. Bai and B. E. Conway, *J. Appl. Electrochem.* **18** (1988) 839.
[7] *Idem, ibid*. **20** (1990) 916.
[8] M. Sloïm, PhD thesis, Université Pierre et Marie Curie, Paris (1975).
[9] S. Virtanen, H. Wojtas, P. Schmuki and H. Böhni. *J. Electrochem. Soc.* **140** (1993) 2786.
[10] N. Hackerman, E. S. Snavely and L. D. Fiel, *Corrosion Sci.* **7** (1967) 39.
[11] A. K. Vijh, in *Electrochemistry of Metals and Semiconductors*, Marcel Dekker, New York (1973).
[12] F. A. Cotton and G. Wilkinson, *in* 'Advanced Inorganic Chemistry', Longmans, London (1986).
[13] H. H. Hyman and J. J. Katz, *in* 'Non-Aqueous Solvent Systems' (edited by T.C. Waddington), Academic Press New York (1965), chapter 2.
[14] A. J. Rudge, *in* 'Industrial Electrochemical Processes' (edited by A.T. Khun) Elsevier, Amsterdam (1971), chapter 1.
[15] J. Devynck, B. Trémillon, M. Sloim and H. Ménard, *J. Electroanal. Chem.* **78** (1977) 355.
[16] S. Dong, Y, Die and G. Cheng, *Electrochim. Acta* **37** (1992) 17.
[17] S. Fletcher, R. G. Barradas and J. G. Porter, *J. Electrochem. Soc.* **125** (1978) 1962.
[18] A. M. Castro Luna de Medina, S. L. Marchiano and A. J. Arvia, *J. Appl. Electrochem.* **8** (1978) 121.
[19] B. Miller, *J. Electrochem. Soc*. **116** (1969) 1675.
[20] D. D. Macdonald, *ibid*. **121** (1974) 651.
[21] W. H. Smyrl, *in* 'Comprehensive Treatise of Electrochemistry', vol. 4 (edited by J. O'M Bockris, B. E. Conway, E. Yeager and R. E. White) Plenum Press, New York (1981) p. 97
[22] U. Bertocci and D. R. Turner, *in* 'Encyclopedia of the Electrochemistry of the Elements', vol. 2 (edited by A. J. Bard) Marcel Dekker, New York (1973).
[23] L. Pauling, *J. Chem. Educ.* **33** (1956) 16.
[24] E. Potvin, M. Drogowska, H. Ménard and L. Brossard, *Can. J. Chem*. **65** (1987) 2109.
[25] J. O'M Bockris and A. K. Reddy, *in* Modern Electrochemistry' vol. 2, Marcel Dekker, New York (1969).
[26] R. D. Peacock, *in* Progress in Inorganic Chemistry', vol.2 (edited by F. A. Cotton) Interscience, New York (1960) p. 193
[27] W. Visscher and E. Barendrecht, *Electrochim. Acta* **25** (1980) 651.
[28] F. Hahn, B. Beden, M. J. Croissant and C. Lamy, *ibid*. **31** (1986) 325.
[29] S. Y. Qian and B. E. Conway, *J. Appl. Electrochem.* **24** (1994) 195.
[30] B. Burrows and R. Jasinski, *J. Electrochem. Soc*. **115** (1968) 348.
[31] W. J. McG. Tegart, *in* 'The Electrolytic and Chemical Polishing of Metals in Research and Industry', Pergamon Press, London (1959), chap 10.
[32] J. S. Clarke and A. T. Khun, *J. Electroanal. Chem.* **85** (1977) 299.
[33] Y. Kansaki and S. Oayagui, *J. Electrochem. Soc.* **36** (1972) 297.
[34] T. Teherani, R. Itaya and A. J. Bard, *Nouv. J. Chim.* **2** (1978) 481.
[35] D. K. Y. Wong, B. A. W. Coller and D. R. Macfarlane, *Electrochim. Acta* **38** (1993) 2121.
[36] L. Brossard, *J. Electrochem. Soc.* **130** (1983) 403.
[37] A. L. Bacarella and J. C. Geiss Jr., *ibid.* **120** (1973) 459.
[38] R. L. Brossard, *Can J. Chem*. **60** (1982) 616.
[39] F. Flade, *Z. Phys. Chem.* **76** (1911) 503.
[40] D. W. Shoesmith and W. Lee, *Electrochim. Acta* **22** (1977) 1411.
[41] H. Dumont, S. Y. Qian and B. E. Conway, to be published.
[42] N. F Mott, *Trans. Faraday Soc.* **35** (1939) 1175.
[43] *Idem, ibid*. **36** (1940) 472.
[44] *Idem, ibid*. **43** (1947) 429.
[45] N. Cabrera and N. F Mott, *Rep. Prog. Phys.* **12** (1949) 163.
[46] B. E. Conway, B. Barnett, H. Angerstein-Kozlowska and B. V. Tilak, *J. Chem. Phys.* **93** (1990) 8361.
[47] P. J. Sonneveld, W. Visscher and E. Barendrecht, *Electrochim. Acta* **37** (1992) 1199.
[48] D. W. Shoeshith, T. E. Rummery, D. Owen and W. Lee, *J. Electrochem. Soc.* **123** (1976) 790.